Lasers in Manufacturing Conference 2021

Plasma dynamics induced by single-pulse femtosecond laser ablation of dielectrics and metals

Bruno Gonzalez-Izquierdo[a], Haruyuki Sakurai[a], Ryohei Yamada[b] , Kuniaki Konishi[a], Makoto Kuwata-Gonokami[b], Junji Yumoto [a,b,*]

[a]*Institute for Photon Science and Technology, The University of Tokyo, 7-3-1 Hongo, Bunkyo-ku, Tokyo,113-0033, Japan*
[b]*Department of Physics, The University of Tokyo, 7-3-1 Hongo, Bunkyo-ku, Tokyo, 113-0033, Japan*

Abstract

The generation of plasma is inherent to subtractive laser processing phenomena and often determines energy absorption and damage characteristics. However, few experimental studies have directly focused on quantitatively analyzing such laser-induced plasma dynamics. Here, shadowgraph and interferogram techniques were combined in a pump-probe configuration to investigate experimentally the temporal (from sub-ps to ns) and spatial dynamics of ablation plasma generated under single-pulse, ultrashort (90-400fs) laser ablation of sapphire and copper. From the measurements, we derived the electron-plasma density and plasma distribution for each time delay. The results clearly reveal time evolution differences between the materials. In sapphire, the plasma expands predominantly perpendicularly to the surface and attains higher electron-plasma densities. In copper, more shocked air-plasma is produced which, instead, expands uniformly. These results provide new insights into the underlying physics of laser-induced plasma dynamics which could facilitate, for instance, the optimization of recent high repetition rate configurations in laser processing.

Keywords: laser-ablation, plasma dynamics, single-pulse, dielectric, metal;

1. Introduction

In the last few decades laser processing techniques have been applied to a wide range of technological fields, from the automotive/aerospace industry to the micro-machining of surfaces in nanotechnology

* Corresponding author. Tel.: +81-3-5841-4082.
E-mail address: yumoto@ipst.s.u-tokyo.ac.jp.

(Schaaf, 2010). Specifically, the use of femtosecond lasers in micro-machining and precision machining processes is nowadays of great interest (Hu, 2020). One of the most important phenomena in the techniques involving ablation and bonding of material is the generation of plasma during the interaction of intense laser beams with matter. The physics of plasma dynamics is complex as it is intrinsically linked to the laser-matter absorption and the electron-plasma density (n_e). Previous experimental studies have been mainly focused on the temporal and spatial evolution of the electron-plasma density and plasma expansion from nanosecond to microsecond time scales (Breitling et al., 1999; Cao et al., 2019) and by using laser pulses of picosecond and nanosecond in duration. However, few experiments investigate the early-stage evolution (from sub-picosecond to a few nanoseconds) of the laser-induced plasma dynamics when using femtosecond laser pulses.

In this paper, we present a qualitative and quantitative experimental characterization of the temporal early-stage (sub-ps to ns), 2D spatial evolution of the ablation plasma dynamics generated in ultrashort (90-400 fs) laser ablation interactions with dielectric (Sapphire) and metal (Cu) targets. The investigation focuses on the measurement of the plasma expansion (by employing a shadowgram configuration) and its corresponding electron-plasma density (by employing a Nomarski interferometer, whose design is detailed in the next section) for each evaluated time step and investigated material. We, therefore, conduct a direct comparison of the plasma dynamics in two of the most representative materials in laser processing applications.

2. Experimental set-up and results

In order to experimentally measure the 2D spatial distribution of the plasma expansion and the electron plasma density, shadowgram and interferometer techniques were employed, respectively, set up in a pump-probe configuration under ambient air environment at atmospheric pressure. The experiment was performed using a Ti:Sapphire laser which delivers linearly(p)-polarized pump pulses with a 5 kHz repetition rate at ~800 nm central wavelength. Single pulses were selected by a combination of an optical chopper and shutter, and focused using a plano-convex lens (L_f, f = 50 mm) to a spot with a minimum diameter equal to ~24 μm at $1/e^2$. Thick (3 mm) planar sapphire and copper targets were employed, with the targets irradiated at normal incidence and with pulse durations of ~90 fs, ~200 fs and ~400 fs. The position of the lens' geometric focus was displaced ~300 μm inwards of the target surface, measuring a peak fluence of ~9.45 Jcm^{-2} at the targets surface. The probe beam was taken as a fraction of the pump beam and doubled in frequency with a BBO crystal. A higher frequency of the probe beam enables the characterization of higher electron plasma densities and eases the suppression of the plasma-scattered light from the pump beam at the detectors (CMOS cameras). The temporal evolution of the plasma dynamics, from sub-ps to few ns, was investigated by inserting an optical delay stage (DS) into the probe beam path. A schematic of the optical setup is shown in Fig. 1(a).

An illustration of the employed shadowgram technique is shown in Fig. 1(b1). Interferometry techniques are based on the spatial and temporal superposition of two (or more) beams, with the same excitation state, forming a fringe pattern at the detector plane. In this investigation, a Nomarski interferometer (Benattar et al., 1979) was selected for its relatively simple design and the absence of alignment to ensure equal optical path length between the two interfering beams at the detector plane. This was accomplished by using a Wollaston prism as a beam splitter, which spatially separates the two orthogonal components of the probe beam within a specific angle (the polarization of the probe beam was rotated at 45°, before entering the Wollaston prism, with a λ/2 waveplate placed before the target). A polarizer device, specifically a Glan-Thompson polarizer, was placed after the Wollaston prism and rotated parallel (or perpendicular) to the polarization of the incident beam ensuring, thus, the same polarization of the two transmitted beams. An

illustration of the employed Nomarski interferometer is shown in Fig. 1(b2). The spatial resolution of the electron density measured with this technique is determined by the quality of the imaging lens (L_i in Fig. 1) and the fringe separation, which can be adjusted by the spacing between the Wollaston prism and L_i.

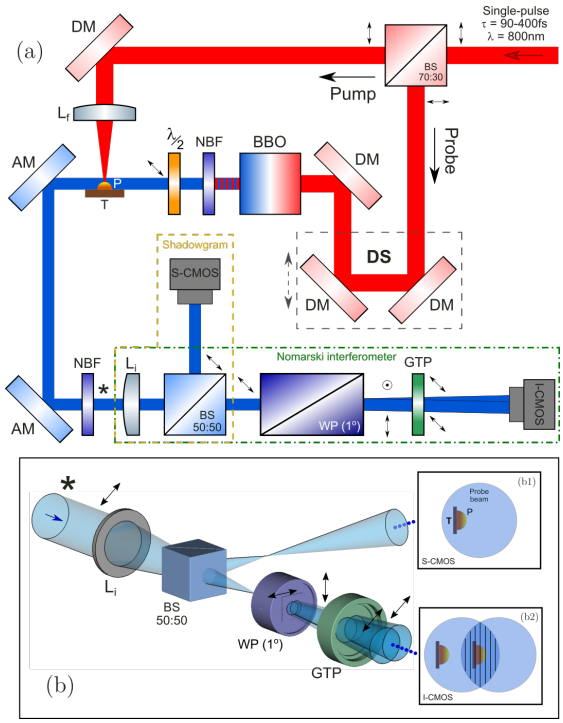

Fig. 1. Conceptual experimental set-up. (a) A Shadowgram and a Nomarsky interferometer were combined in a pump-probe configuration. Temporal evolution (from ps to ns) of plasma dynamics was investigated by using a delay stage (DS). (b) 3D scheme of the shadowgram and the Nomarski interferometer shown in (a); (b1) Illustration of the plasma shadowgram recorded by the S-CMOS camera; (b2) Illustration of the plasma interferogram recorded by the I-CMOS camera. Two overlapping images, at the same excitation state, interfere constructively at the camera position generating a fringe pattern. The asterisk symbol (*) in (a) and (b) corresponds to the same physical position at the setup. Black double-arrows indicate the polarization state of the laser beam at each location of the setup. BS: Non-polarized beam-splitter; λ/2: half-lambda waveplate; GTP: Glan-Thompson polarizer; DM: Dielectric mirror; L_f: focusing lens (f = 50 mm); L_i: imaging lens (f = 100 mm); BBO: Barium borate crystal; NBF: Narrow band-pass filter (centered at 2ω [400 nm]); AM: Aluminum mirror; WP: Wollaston prism; S-CMOS: CMOS camera for shadowgraphy; I-CMOS: CMOS camera for interferometry; P: Ablation plasma; T: Target.

In presence of a spatially varied refractive index (η), as in a plasma, a phase shift (ϕ) of the initial beam is induced, producing, in turn, a modulation of the fringes separation in an interferogram (Takeda et al., 1982). Assuming an axial symmetry of the plasma distribution, the refractive index is determined by the Abel inversion of the induced phase shift (Hutchinson, 2002). Although different species of plasma particles (such as free-electrons and heavy ions) could contribute to the refractive index distribution, in this investigation we expect a dominant role of the free-electrons for the majority of the plasma structures (in the same way as discussed in Breitling et al., 1999 or Wei et al., 2014). In this case, the electron-plasma density is related to the plasma refractive index by the Drude's model as follow:

$$n_e(r) = n_c(\lambda) \cdot [1 - \eta^2(r)] \quad (1)$$

where n_c is the critical electron density [$n_c(cm^{-3}) \sim 1.1x10^{21}/\lambda^2(\mu m)$], defined as the electron density when the plasma frequency is equal to the laser frequency, and λ is the wavelength of the interfered beam.

Although interferometry techniques are a robust tool for estimating the electron plasma density, they present a lower detection limit of the electron plasma density (~10^{18} cm^{-3}) due to the minimum detectable fringe-shift, and an upper detection limit defined by the critical electron density, n_c (~$6.98x10^{21}$ cm^{-3} at λ = 400 nm) in addition to refraction and absorption effects. However, for the laser parameters and experimental conditions used in the present investigation this method is applicable since the electron plasma density lies within the mentioned boundaries (see experimental results in the following subsections).

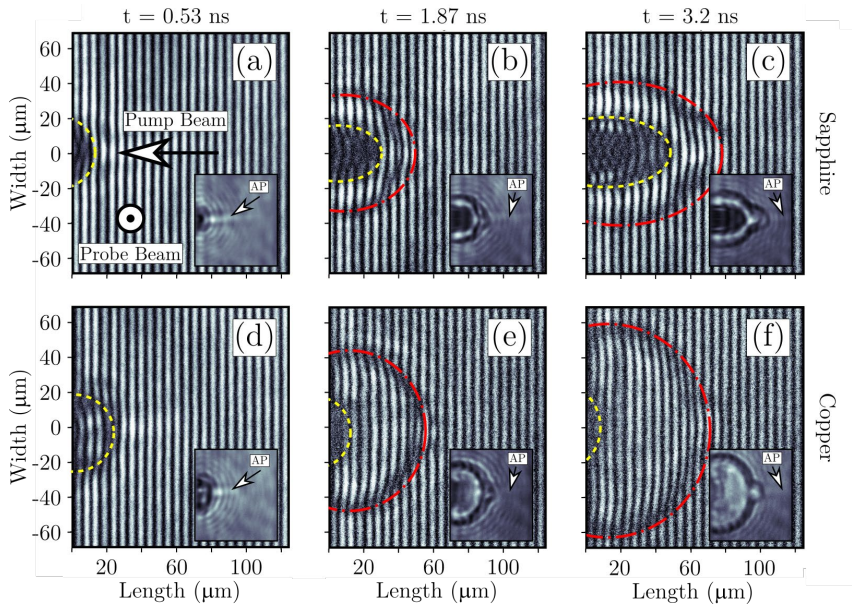

Fig. 2. Representative interferograms measured experimentally. (a)-(c) Temporal snapshots at t = 0.53 ns, t = 1.87 ns and t = 3.2 ns respectively (t = 0 ns is defined as the instant when the pump beam hits the target surface) in sapphire for a pulse duration of τ ~200 fs; (d)-(f) same as (a)-(c) but in copper. The main plasma plume is separated from the shocked air-plasma through the contact front (yellow-dashed line). The red-dash-dotted line corresponds to the shockwave front. Target surface is located at Length = 0 μm. The corresponding shadowgrams are included inset. AP: Air plasma generated by the pump laser beam.

2.1. Temporal plasma distribution

Representative interferograms measured experimentally for a single pump beam interacting in sapphire with a pulse duration of τ ~200 fs are shown in Fig. 2(a-c). This figure displays a time evolution of the 2D spatial distribution of the plasma formation and expansion for a time delay equal to t = 0.53 ns (Fig. 2(a)), t = 1.87 ns (Fig. 2(b)) and t = 3.2 ns (Fig. 2(c)), where t = 0 ns was defined as the instant when the pump beam hits the target surface. They clearly show a shift in the fringes' separation where spatial variations of the plasma refractive index are presented. The darker areas denote a presence of higher electron densities where absorption effects of the probe beam are more pronounced. This fact is more evident in the corresponding shadowgrams, included inset. At the earliest time (Fig. 2(a)), only the main plasma plume (MPP) and air plasma (AP), generated both by the pump laser beam, are presented. Later in time (Fig. 2(b)), the ablated material, expanding in a supersonic regime, produces a shockwave (Campanella et al., 2019) propagating in and partially ionizing the surrounding ambient gas (SAP). The shockwave front is delimitated with a red-dash-dotted line in Fig. 2. As a result, two layers separated by a contact front (yellow-dashed line

in Fig. 2) are formed, which correspond to the MPP and an enclosing shocked layer comprising of ionized ambient gas. At the last point in time (Fig. 2(c)), MPP exhibits an expansion predominantly perpendicular to the target surface and with a bulge formed at the front of the SAP layer. This bulge formation has been reported in the past in other target materials (Breitling et al., 1999; Zhang et al., 2015), and explained as the result of the interaction of the SAP layer and the air-plasma channel. In Fig. 2(d-f) the measured interferograms corresponding to laser ablation plasma in copper at the same time delays as in Fig. 2(a-c) are shown.

One of the more salient differences in terms of plasma generation and plasma expansion between sapphire and copper is that the MPP is significantly larger at the earliest investigated time delay (t = 0.53 ns) in copper, and that its expansion is more pronounced parallel to the target surface. This figure also shows that the size of the MPP layer increases with time in sapphire, whereas in copper, the size of the MPP is maximum at the earliest shown time delay (t = 0.53 ns) and decreases continuously within the limits of our observation, until a time delay of t = 3.2 ns (most probably because of the electron-ion recombination mechanism). Because of this, a larger SAP layer, in proportion to the MPP, is generated in copper compared to sapphire.

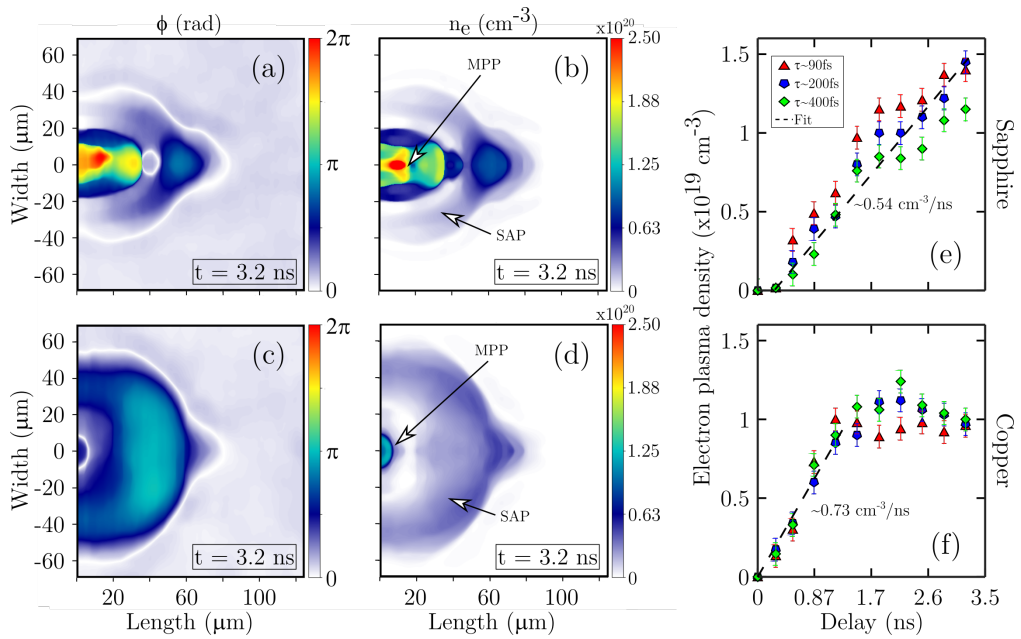

Fig. 3. (a,b) 2D map of the phase shift, ϕ (absolute value) and the electron plasma density, n_e, respectively, in sapphire at t = 3.2 ns and pulse duration τ ~200 fs, calculated from the interferogram shown in Fig.2(c); (c,d) same as (a,b) but in copper and calculated from the interferogram shown in Fig.2(f); Target surface is located at Length = 0 μm. (e,f) Temporal evolution of the spatially-averaged electron plasma density in sapphire and copper, respectively, for the stated pulse durations. The error bars were estimated from four individual shots measured at t = 3.2 ns and with the same initial laser parameters. MPP: Main plasma plume; SAP: Shocked air plasma.

2.2. Temporal electron plasma density

As explained above, the electron plasma density can be retrieved from the measured interferograms. To do so, first, the induced phase shift is calculated by using the method explained in Takeda et al., 1982. Fig. 3(a) and 3(c) shows the calculated 2D map of the phase shift in sapphire (corresponding to the interferogram from Fig. 2(c)) and copper (corresponding to the interferogram from Fig. 2(f)), respectively. Assuming an axial

symmetry, the spatial distribution of the refractive index is determined by applying the Abel inversion to the phase shift map. Finally, the electron plasma density is determined by replacing the refractive index values into the equation (1). Fig. 3(b) and Fig. 3(d) show the corresponding electron plasma density in sapphire and copper, respectively, for the illustrated example. They show a clear difference in terms of electron plasma density and plasma distribution. A denser and larger MPP is measured in sapphire compared to copper, with a proportionally larger SAP in the case of copper. In average the electron density in the SAP layer is slightly higher in copper than in sapphire, and its value is around 3.5 times lower than the density in the MPP for copper and around one order of magnitude lower for sapphire. We also noticed that in sapphire the presence of the bulge at the front of the SAP structure generates a locally denser plasma region compare to the rest of SAP layer.

The spatially-averaged value of the total electron plasma density (i.e. including MPP and SAP) as a function of the probe-delay for the three investigated pump-pulses durations (τ ~90 fs, τ ~200 fs and τ ~400 fs) for sapphire and copper are respectively plotted in Fig. 3(e) and 3(f). The error bars were estimated from four individual shots measured at t = 3.2 ns using the same initial laser parameters. Fig. 3(e) and 3(f) show a clear difference in the generation and evolution of the laser ablation plasma in the two investigated materials. The expansion of plasma in sapphire is delayed by about ~0.2 ns compared to the plasma in copper, which exhibits a significant expansion and electron density value at that time delay. The rate of free-electron generation (cm^{-3}/ns) is near constant during the investigated probe delay, whereas in copper it remains constant up to ~1.5 ns from where it saturates and reduces almost to 0 cm^{-3}/ns. In addition, the rate of free-electron generation is significantly higher in copper than in sapphire up to ~1.5 ns. Above ~1.5 ns the electron density is higher for the shortest pulse durations (τ ~90 fs) in sapphire, whereas the opposite seems to be in copper.

3. Conclusions

The temporal (from sub-ps to ns) and spatial dynamics of ablation plasma generated under single-pulse, ultrashort (90-400 fs) laser ablation in sapphire and copper have been investigated experimentally. The evolution of the electron plasma density and the plasma distribution were quantitatively derived using a combination of interferogram and shadowgraphy techniques arranged in a pump-probe configuration. Distinctive differences were measured in the two investigated materials. In copper, plasma begins to expand earlier in time and with higher values of the electron plasma density rate. However, above ~1.5 ns, additional electrons are not generated anymore whereas in sapphire the electron plasma density rate keeps almost constant during the studied time window (up to ~3.2 ns). Additional experiments as well as theoretical and simulation studies are required to elucidate additional understanding of this particular behavior of the electron plasma density evolution in sapphire. A slight effect of the pump-beam pulse duration on the free-electron plasma generation was measured. In sapphire, the electron plasma density is slightly higher for the shortest pulse duration (~90 fs) for all the investigated time delays. On the contrary, copper plasma shows slightly higher values of the electron density for the longest pulse duration (~400 fs), and being only appreciated above ~1.5 ns time delay. In terms of plasma expansion, the main plasma plume in sapphire expands predominantly in the direction that is perpendicular to the target surface and produces a proportional shocked air plasma in size around it. In copper, in turn, the main plasma plume expands more into the direction that is parallel to the target surface and, a much larger shocked air plasma layer, in proportion compared to the sapphire case, is generated.

These experimental results demonstrate that different target materials exhibit particular temporal responses to the interaction of ultrashot single laser pulses and provide new insights into the underlying

physics of laser-induced plasma dynamics for each investigated case, which in turn could facilitate, for instance, the optimization of recent high repetition rate configurations in laser processing.

Acknowledgements

We thank the Center of Innovation Program funded by the Japan Science and Technology Agency (JST).

References

Benattar, R., Popovics, C., Sigel, R., 1979. Polarized light interferometer for laser fusion studies, Review of Scientific Instruments 50, p. 1583-1586.

Breitling, D.; Schittenhelm, H.; Berger, P.; Dausinger, F. & Hügel, H., 1999. Shadowgraphic and interferometric investigations on Nd:YAG laser-induced vapor/plasma plumes for different processing wavelengths, Applied Physics A: Materials Science & Processing 69, p.505-508.

Campanella, B., Legnaioli, S., Pagnotta, S., Poggialini, F., Palleschi, V., 2019. Shock Waves in Laser-Induced Plasmas, Atoms, MDPI AG 7, p. 57.

Cao, S., Su, M., Min, Q., Sun, D., Ma, P., Wang, K., Jiao, Z., Dong, C., 2019. Dynamics and density distribution of laser-produced Al plasmas using optical interferometry and optical emission spectroscopy, Journal of Quantitative Spectroscopy and Radiative Transfer 225, p. 69-75.

Hu, A. (Ed.) 2020. Laser Micro-Nano-Manufacturing and 3D Microprinting, Springer.

Hutchinson, I. H., 2002. Principles of Plasma Diagnostics, Cambridge University Press, p. 141.

Schaaf, P., 2010. Laser Processing of Materials: Fundamentals, Applications and Developments, Springer.

Takeda, M., Ina, H., Kobayashi, S., 1982. Fourier-transform method of fringe-pattern analysis for computer-based topography and interferometry, Journal of the Optical Society of America 72, p. 156.

Wei, W., Li, X., Wu, J., Yang, Z., Jia, S., Qiu, A., 2014. Interferometric and schlieren characterization of the plasmas and shock wave dynamics during laser-triggered discharge in atmospheric air, Physics of Plasmas 21, p. 083112.

Zhang, H., Zhang, F., Du, X., Dong, G., Qiu, J., 2015. Influence of laser-induced air breakdown on femtosecond laser ablation of aluminum, Optics Express 23, p. 1370.